This article has been accepted for publication in a future issue of this journal, but has not been fully edited. Content may change prior to final publication. Citation information: DOI 10.1109/ACCESS.2021.3101441, IEEE Access

IEEE Access
Multidisciplinary | Rapid Review | Open Access Journal

Date of publication xxxx 00, 0000, date of current version xxxx 00, 0000.
Digital Object Identifier 10.1109/ACCESS.2017.Doi Number

Wideband Circularly Polarized Textile MIMO Antenna for Wearable Applications

Sanjeev Kumar[1], Durgesh Nandan[2], Kunal Srivastava[3], Sachin Kumar[4], Hari Singh[5], Mohamed Marey[6], Hala Mostafa[7], and Binod Kumar Kanaujia[8]
[1, 2]Accendere Knowledge Management Services Pvt. Ltd. (CL Educate Ltd.), India
[3, 5, 8]School of Computational and Integrative Sciences, Jawaharlal Nehru University, New Delhi 110067, India
[4]Department of Electronics and Communication Engineering, SRM Institute of Science and Technology, Chennai 603203, India
[6]Smart Systems Engineering Laboratory, College of Engineering, Prince Sultan University, Riyadh 11586, Saudi Arabia
[7]Information Technology Department, College of Computer and Information Sciences, Princess Nourah bint Abdulrahman University, Riyadh 84428, Saudi Arabia

Corresponding author: Sachin Kumar (gupta.sachin0708@gmail.com).

The authors would like to acknowledge the support of Prince Sultan University for paying the Article Procesfsing Charges (APC) of this publication.

ABSTRACT In this paper, a wideband circularly polarized (CP) textile multiple-input-multiple-output (MIMO) antenna is presented for wearable applications. The designed MIMO antenna consists of two sickle-shaped resonating elements and a common ground plane. Each antenna element is excited by a microstrip line feed, and an inverted L-shaped strip is introduced in the ground plane to support circular polarization. The antenna covers impedance bandwidth (S_{11}≤–10 dB) of 3.6–13 GHz and 3-dB axial ratio bandwidth (ARBW) of 5.2–7.1 GHz. The proposed textile MIMO antenna exhibits envelope correlation coefficient (ECC) <0.02, diversity gain (DG) >9.96, total active reflective coefficient (TARC) <-10 dB, channel capacity loss (CCL) <0.2 b/s/Hz, and mean effective gain (MEG) ratio within ±0.5 dB. The antenna offers dual-sense circular polarization and high isolation (>18) between the resonating elements. Also, the proposed antenna is investigated for different human body situations, and its specific absorption rate (SAR) for human tissues specimen is studied. The overall size of the proposed CP textile MIMO antenna is 32.5×42×1 mm^3. The designed MIMO antenna could be useful for wearable applications due to its textile layers, reasonable on-body performance, and compact size.

INDEX TERMS bending, circular polarization, isolation, textile antenna, wearable

I. INTRODUCTION

Recently, wearable gadgets have received considerable attention from designers due to their widespread applications in healthcare, entertainment, navigation, remote monitoring, rescue, and security [1–2]. An antenna is an important element of a wearable transceiving system. Wearable/textile antennas are needed to radiate efficiently in a number of situations such as body gestures, bending, running, and movement. Textile antennas must be low-profile, conformal, light in weight, flexible, robust, and compact in order to be easily integrated into portable electronic devices or clothing [3]. Antennas designed for wearable applications are intended to operate in close proximity to the human body. Therefore, several issues must be considered during the textile antenna design process, such as structural deformation, antenna placement, and fabrication [4–5]. Wideband circularly polarized (CP) antennas are attractive candidates for wearable applications due to their orientation flexibility, better mobility, and multipath interference suppression capability [6–8]. Multiple-input-multiple-output (MIMO)/diversity technology is also gaining popularity for improving link capacity, particularly in complex multipath environments. A multi-element antenna with polarization diversity is a good choice for encountering multipath fading and establishing reliable channels [9–11].

Many wearable MIMO antennas with high inter-element isolation have been presented in the literature [12–17]. In [12], a dual-band textile-based MIMO antenna was proposed for WLAN applications, where vias were used to modify the resonant mode of the waveguide cavity. A circular-shaped MIMO antenna with high impedance surface (HIS) was reported [13], where isolation larger than 15 dB was achieved between the ports. A solo-coat textile

IEEE Access Multidisciplinary ⋮ Rapid Review ⋮ Open Access Journal

MIMO antenna was presented for wearable applications [14], where the ground plane worked as the radiator. In [15], a two-element wearable MIMO antenna was reported for ultra-wideband (UWB) applications, where a partially suppressed ground plane was used to obtain isolation >26 dB. A wideband rectangular-shaped textile MIMO antenna was presented in [16], where two I-shaped stubs were used to achieve high inter-element isolation.

Over the last five years, a few CP MIMO antenna designs have been developed that can be used for WLAN, C-band, and satellite applications [17–21]. In [17], a coplanar waveguide (CPW)-fed square slot MIMO antenna was presented, where inverted-L planar strips were used in the ground plane to obtain wide axial ratio bandwidth (ARBW). A dual CP antenna was reported in [18], where a combination of L-shaped strips was used to obtain circular polarization. In [19], a CP MIMO antenna consisted of grounded stubs and a mirrored F-shaped defected ground structure (DGS) in the ground plane was proposed. In [20], a CP antenna with monopole extension of the microstrip line was presented, where the orthogonal fields are induced through the modified ground plane. In [21], a CP MIMO antenna was presented for wearable gadgets, where the phase difference between orthogonal modes can be controlled by a metal strip loaded in the ground plane. The MIMO antennas presented in [12–16] showed linearly polarized (LP) characteristics while the antennas in [17–21] showed CP performance. Most of the wearable/textile antennas reported in the available literature are LP single element configurations with narrow ARBW, and wearable CP MIMO antenna with wide ARBW is rarely reported.

In this article, a low-profile compact-sized two-element CP MIMO textile antenna is presented for wearable applications. The proposed MIMO antenna element consists of a microstrip line-fed sickle-shaped radiator and a modified ground plane. An L-shaped stub is integrated with the modified ground plane to introduce a quadrature phase shift between the horizontal and vertical electric field vectors. The two identical antenna elements are located in a mirrored-image fashion to obtain dual-sense radiation characteristics. Port-1 emits left-hand CP (LHCP) waves while port-2 emits right-hand CP (RHCP) waves. This property makes the proposed MIMO antenna suitable for polarization diversity operation.

II. ANTENNA CONFIGURATION

A. ANTENNA ELEMENT DESIGN

Fig. 1 shows the geometric layout of the proposed CP textile antenna element. The physical size of the antenna element is 20×30.5 mm^2. The antenna element consists of a sickle-shaped radiating patch and a modified ground plane designed on the upper and lower sides of the dielectric substrate, shown in Figs. 1(a) and (b), respectively. A 50 Ω microstrip line is used for feeding the radiator. The simulations of the proposed antenna are performed in ANSYS HFSS® software.

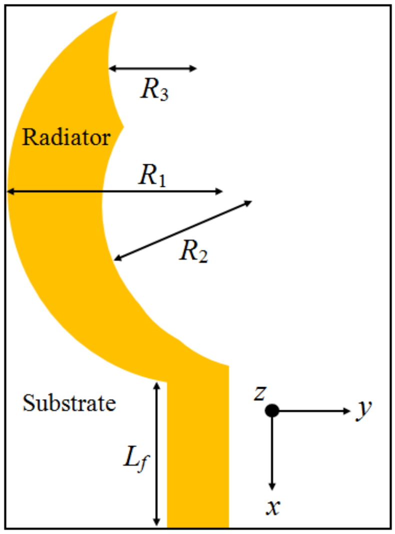

(a)

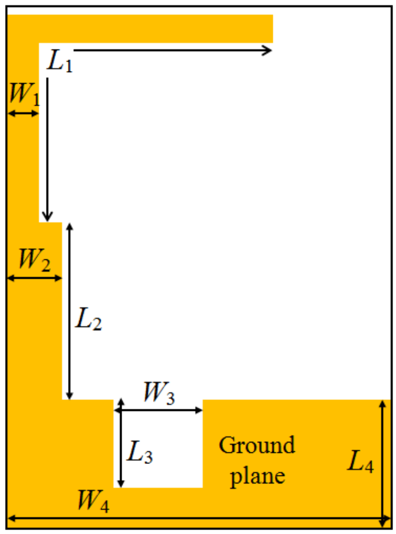

(b)

FIGURE 1. Proposed CP textile antenna: (a) top layout, (b) bottom layout.

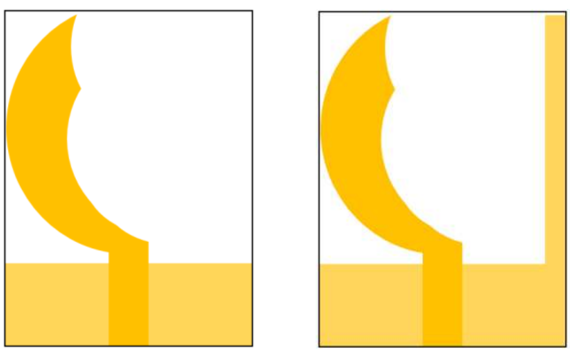

(a) (b)

This article has been accepted for publication in a future issue of this journal, but has not been fully edited. Content may change prior to final publication. Citation information: DOI 10.1109/ACCESS.2021.3101441, IEEE Access

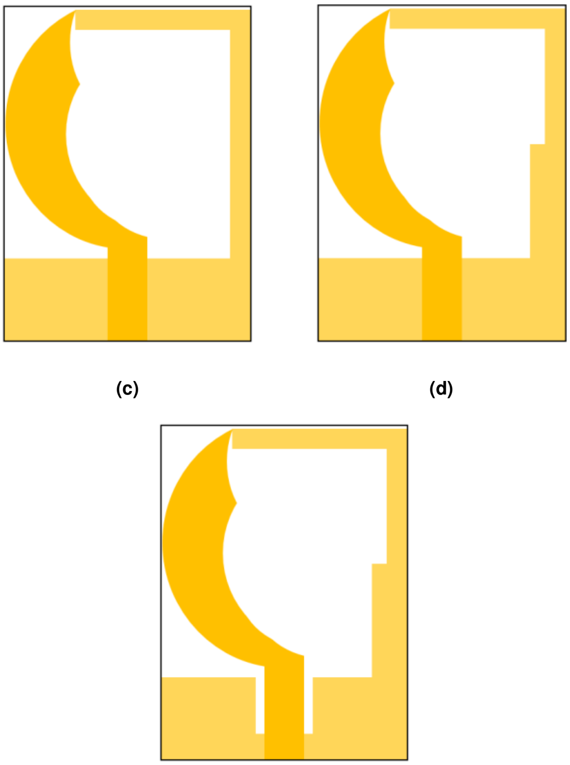

(c) (d)

(e)

FIGURE 2. **Evolution of the proposed textile antenna: (a) Ant. 1, (b) Ant. 2, (c) Ant. 3, (d) Ant. 4, (e) Ant. 5.**

The antenna element is developed on Felt substrate material of thickness of 1 mm, dielectric constant of 1.34, and loss tangent of 0.02. The radiating patch and the ground plane are formed using Sheildit Superconductive material of thickness of 0.17 mm and surface resistivity of <0.5 Ω per square. The design parameters of the antenna element are: R_1=11.5 mm, R_2=10.3 mm, R_3=13.8 mm, L_f =10.2 mm, L_1=23.4 mm, W_1=1.7 mm, L_2=10.5 mm, W_2=3 mm, L_3=5.7 mm, W_3=5 mm, L_4=7.7 mm, W_4=20 mm.

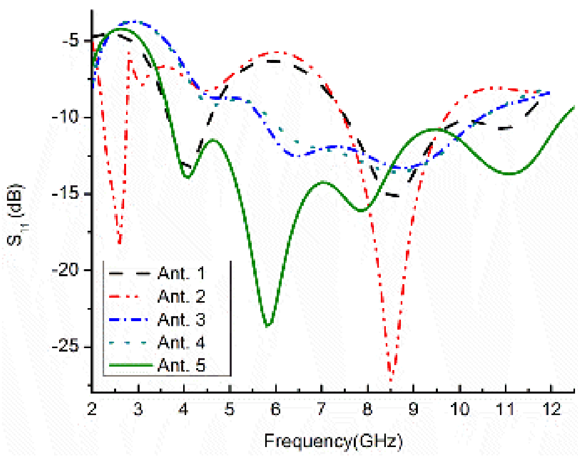

(a)

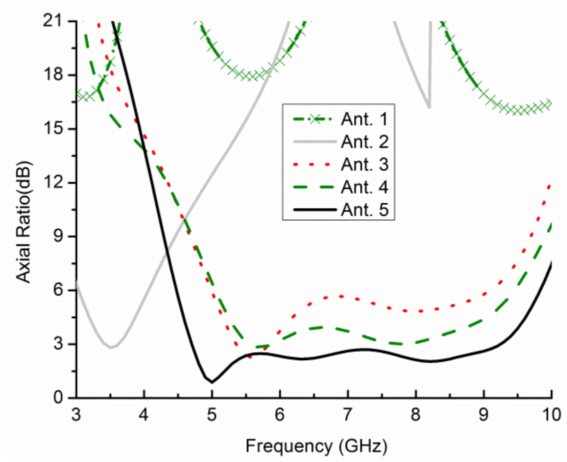

(b)

FIGURE 3. **Simulation results of the design steps: (a) reflection coefficients, (b) axial ratio.**

TABLE I
SIMULATED RESULTS OF THE DESIGN STAGES

Step	Bandwidth (GHz)	Fractional bandwidth (%)	ARBW (GHz)
Ant. 1	3.6–4.5, 7.5–11.3	22.22, 25.24	---
Ant. 2	2.21–2.87, 7.4–9.6	16.6, 16.54	---
Ant. 3	5.5–10.4	64.15	5.3–5.8
Ant. 4	5.8–10.6	58.53	5.5–5.9
Ant. 5 (Proposed)	3.7–12.2	106.91	4.7–9.2

1) DESIGN PROCESS

Fig. 2 presents the evolution process of the textile antenna element. The simulated reflection coefficients and axial ratio curves of the design steps are shown in Figs. 3(a) and (b), respectively. In Fig. 2(a), a microstrip line-fed sickle-shaped radiator is designed on the top of the textile-based substrate material, and a partial ground plane on the bottom of the substrate material. The Ant. 1 shows resonating bandwidth of 3.6–4.5 GHz and 7.5–11.3 GHz. In step-2, as shown in Fig. 2(b), a strip of $\lambda/2$ wavelength is introduced in the partial ground plane to improve impedance bandwidth. Ant. 2 also shows two resonating bands.

Furthermore, as shown in Fig. 2(c), the impedance mismatching is encountered by introducing an L-shaped strip in the ground plane (Ant. 3). The L-shaped strip also induces quadrature phase difference between the two electric field vectors (E_x and E_y). The impedance bandwidth and axial ratio bandwidth (ARBW) of the Ant. 3 are 5.5–10.4 GHz and 5.3–5.8 GHz, respectively. In step-4, the L-shaped strip is alienated into two parts (of dimensions $L_2 \times W_2$ and $L_1 \times W_1$), as shown in Fig. 2(d), which improves the axial ratio of the antenna element (Ant. 4). The antenna resonating band needs to shift to the left side for covering the lower frequency range. For this reason, a rectangular slot (of dimensions $L_3 \times W_3$) is etched from the ground plane

IEEE Access
Multidisciplinary ⋮ Rapid Review ⋮ Open Access Journal

of the antenna element as shown in Fig. 2(e). Thus, the current path length increases and shifts the operating frequency band towards the lower side. Also, superior CP performance is obtained in the proposed Ant. 5. The simulated results (impedance bandwidth and ARBW) of the design stages are listed in Table I.

2) CP PERFORMANCE

Fig. 3(b) shows axial ratio and frequency variations for different stages of the proposed antenna. Ant. 1, shown in stage-1, is LP as the phase difference between the electric field vectors is not 90°. Similarly, Ant. 2 is also LP. Further, L-shaped strip of different lengths and widths are connected to the rectangular ground plane (Ant. 3 and Ant. 4) to achieve 90° phase difference between the electric field vectors. By using this method, the amplitude of E_x and E_y becomes almost equal with 90° phase difference between them [17]. The surface current distributions of the proposed textile antenna (at ωt=0°, ωt=90°, ωt=180°, and ωt=270°) are shown in Fig. 4. A_1 and A_2 symbolize the orthogonal current vectors, and A_3 represents their sum. At ωt=0°, the surface current density on the upper part of the patch (A_1) and the edge of the L-shaped strip (A_2) increases, and the sum (A_3) of these two vectors is heading towards the upper right, shown in Fig. 4(a). At ωt=90°, as displayed in Fig. 4(b), the vector sum A_3 is heading towards the lower right, which illustrates that the current vectors are rotating clockwise as time progresses.

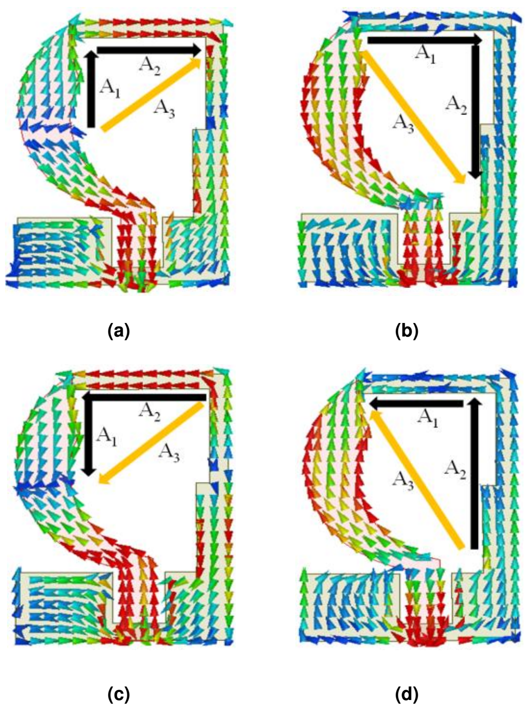

FIGURE 4. Vector current distribution at 5.3 GHz: (a) 0°, (b) 90°, (c) 180°, (d) 270°.

Similarly, at ωt=180° and 270°, the sum (A_3) travels in the clockwise direction as displayed in Figs. 4(c) and (d), respectively. Therefore, the proposed textile antenna demonstrates LHCP operation in the broadside direction.

The $|E_x/E_y|$ and phase difference plots of the proposed Ant. 5 and Ant. 1 are shown in Figs. 5(a) and (b), respectively. The curves reveal that the L-shaped strip on the ground plane balances the magnitude of horizontal and vertical electric field vectors and introduces a 90° phase difference between them. The current path increases by etching a rectangular slot from the ground plane, hence shifting the resonating frequency band towards the left side.

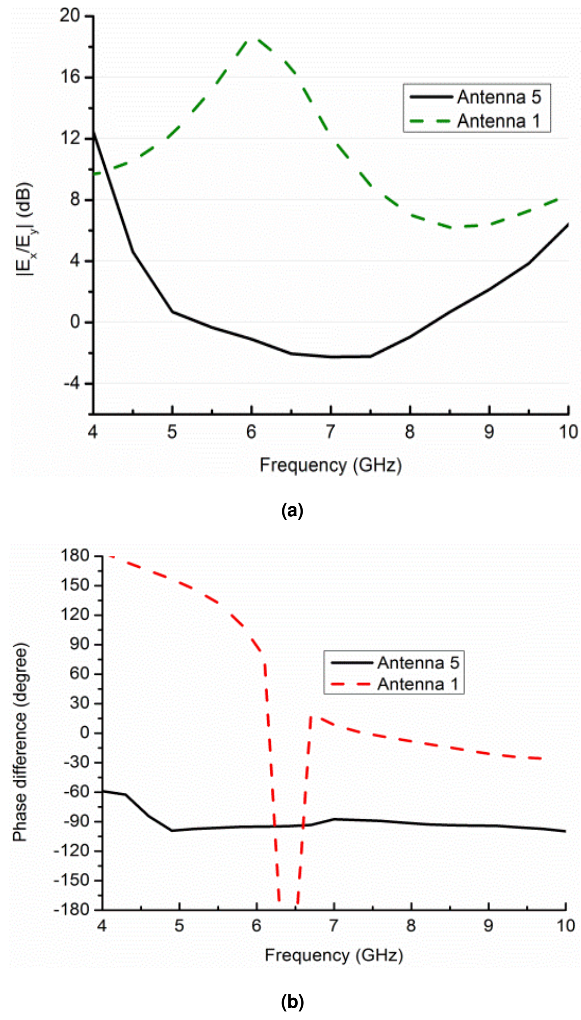

FIGURE 5. Comparison between the Ant. 1 and Ant. 5: (a) $|E_x/E_y|$, (b) phase difference.

B. MIMO ANTENNA

Fig. 6 displays the proposed textile MIMO antenna configuration, where two identical antenna elements (Ant. 5) are placed in a mirrored-image fashion. The monopole radiators are excited through 50 Ω microstrip lines. On the back side of the textile substrate, a shared ground plane is designed with the mirrored L-shaped strips. The proposed CP MIMO antenna parameters are: L_m=32.5 mm, W_m=42

This article has been accepted for publication in a future issue of this journal, but has not been fully edited. Content may change prior to final publication. Citation information: DOI 10.1109/ACCESS.2021.3101441, IEEE Access

mm, L_g=7.2 mm, l_s=16.5 mm, w_s=1 mm, l_5=27.8 mm, w_5=1.2 mm, l_6=9.5 mm, w_6=6 mm, l_7=5.7 mm, w_7=5 mm, w_{12}=1.7 mm, d_1=14.2 mm. The overall size of the proposed textile MIMO antenna is 42×32.5 mm^2. The top and bottom of the textile MIMO antenna prototype are shown in Figs. 6(c) and (d), respectively.

1) DESIGN PROCESS

Due to the mirrored-image arrangement, the L-shaped strips of the antenna elements unite to form a T-shaped stub at the middle of the MIMO Antenna A as shown in Fig. 7(a). Without any decoupling element between the antenna elements, the S_{12} parameters of the presented MIMO antenna are stable. The S-parameters and axial ratio curves of the MIMO Antenna A and MIMO Antenna B are displayed in Figs. 8(a) and (b), respectively. The T-shaped stub between the antenna elements offers isolation >16 dB. However, the ARBW of the antenna changes significantly due to the surface wave coupling. Therefore, a rectangular slot (of size l_s×w_s mm^2) is etched from the T-shaped stub of the MIMO Antenna A to improve 3-dB ARBW of the antenna as shown in Fig. 7(b) (MIMO Antenna B). The slot also improves isolation (>18.5 dB) of the MIMO antenna. The dimensions of the rectangular slot are optimized to realize a wider ARBW. The simulated impedance bandwidth and ARBW of the proposed MIMO Antenna B are listed in Table II.

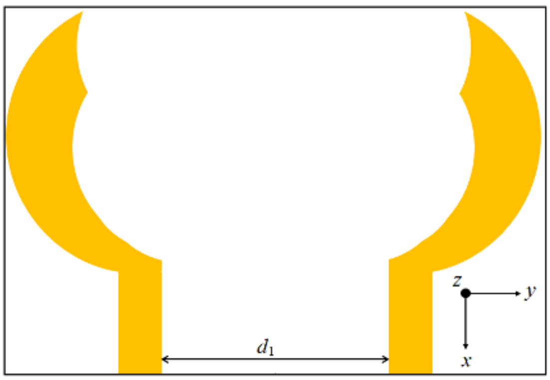

(a)

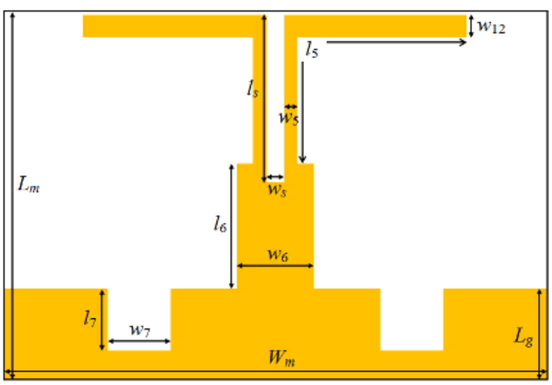

(b)

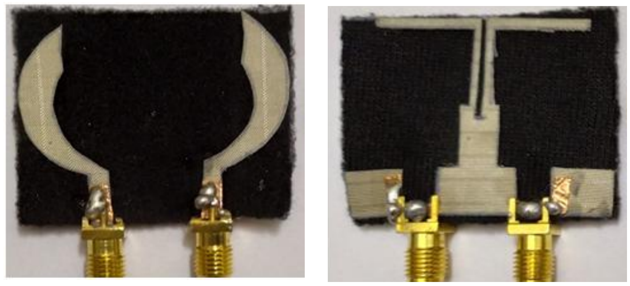

(c) (d)

FIGURE 6. Proposed CP textile MIMO antenna: (a) top view, (b) back view, (c) top view of the fabricated prototype, (d) bottom view of the fabricated prototype.

TABLE II
SIMULATED RESULTS OF THE MIMO ANTENNA B

	ARBW	S_{11}
Operating frequency (GHz)	5–7.3	3.3–13.6
Size (mm^2)		42×32.5
Substrate thickness	1 mm	ε_r=1.34, tan δ=0.02

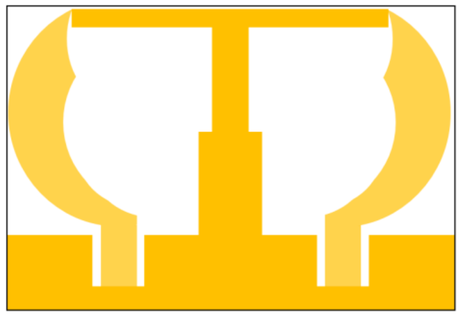

(a)

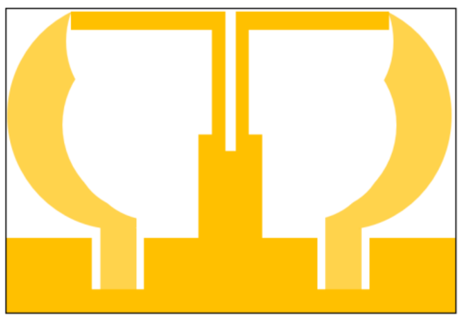

(b)

FIGURE 7. Design of: (a) MIMO Antenna A, (b) MIMO Antenna B.

Fig. 8(c) shows the simulated axial ratio beamwidth of the proposed MIMO antenna at 6 GHz in the $\phi = 0^{\circ}$ and $\phi = 90^{\circ}$ planes. It can be seen that the 3-dB axial ratio beamwidth ranges from -63° to 72° for $\phi = 0^{\circ}$ and -68° to -62° for $\phi = 90^{\circ}$. The simulated and measured efficiency of the proposed antenna are shown in Fig. 8(d), and the peak efficiency is about 78 % at 9.5 GHz. The efficiency is low due to the dielectric loss, smaller surface area, and compact size of the antenna.

2) DUAL-SENSE CP PERFORMANCE

The proposed two-port textile MIMO antenna demonstrates dual-sense radiation characteristics.

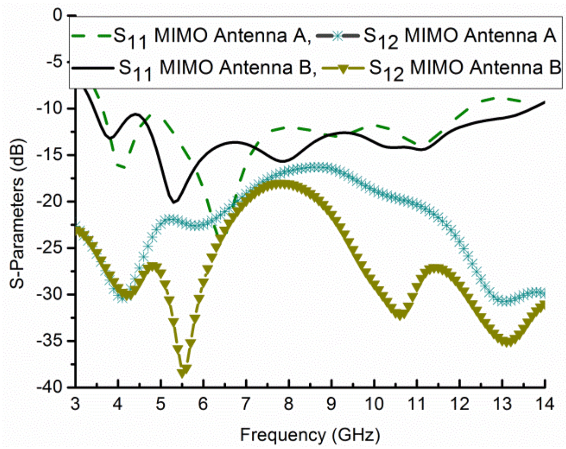

(a)

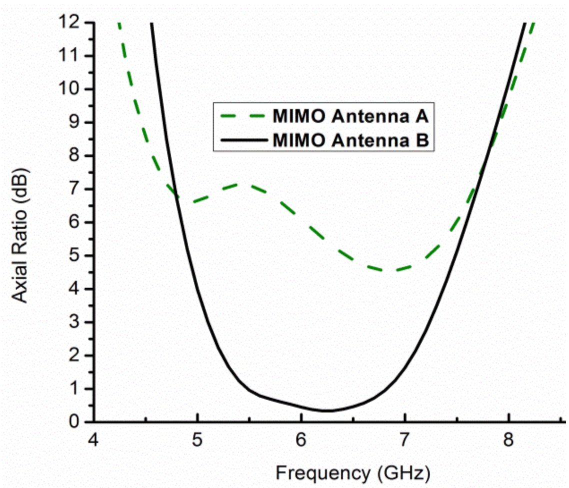

(b)

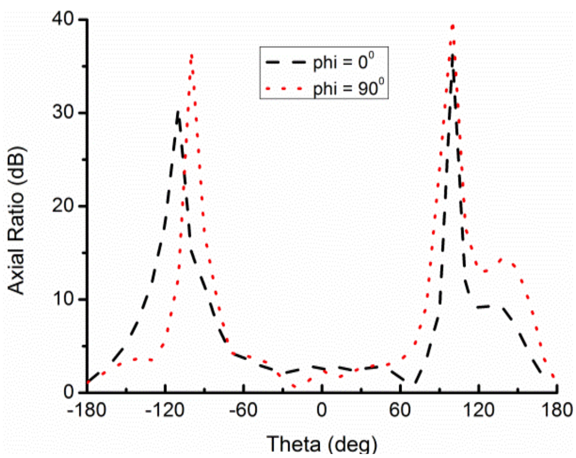

(c)

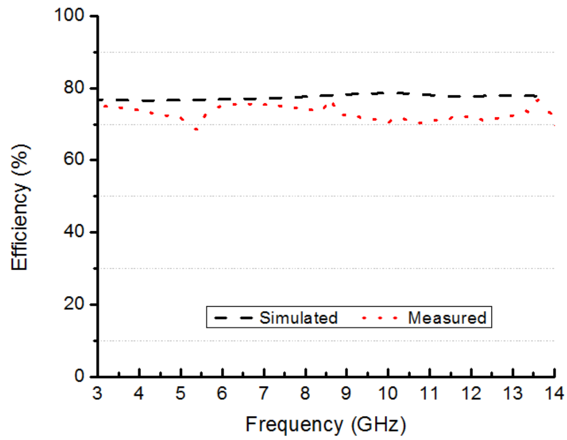

(d)

FIGURE 8. **Simulated response of the textile MIMO antenna: (a) S-parameters, (b) axial ratio, (c) axial ratio beamwidth, (d) antenna efficiency.**

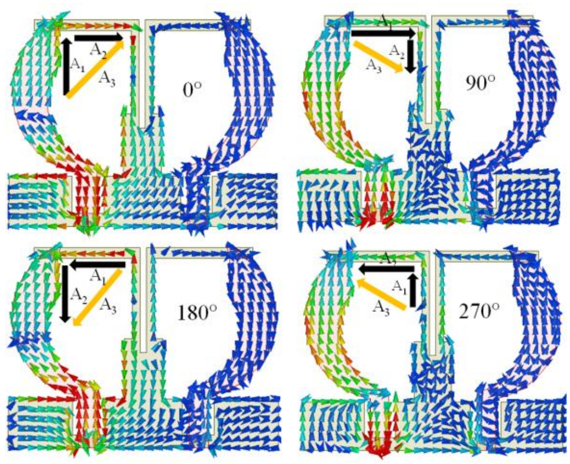

(a)

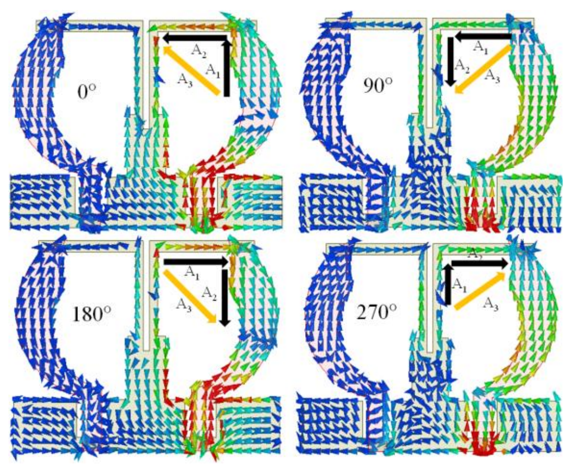

(b)

FIGURE 9. **Surface current distribution at 5.3 GHz: (a) port-1/LHCP, (b) port-2/RHCP.**

The surface current distributions of the textile antenna (at

ωt=0°, ωt=90°, ωt=180°, and ωt=270°) are shown in Fig. 9. Here, A_1 and A_2 symbolize the orthogonal current vectors, and A_3 represents their sum. By changing the port excitation, either LHCP or RHCP behavior can be generated in the broadside direction of the antenna. Figs. 9(a) and (b) illustrate clockwise and anti-clockwise movement of the electric field vectors at port-1 and port-2, respectively. As shown in Fig. 9(a), the resultant (A_3) is heading towards the upper right at ωt=0°, while the vector sum (A_3) is heading towards the lower right at ωt=90°. On the contrary, in Fig. 9(b), the vector sum (A_3) is heading towards the upper left at ωt=0°, while the sum (A_3) is heading towards the lower left at ωt=90°. When port-1 is excited, port-2 is terminated with a load of 50 Ω and vice versa. The simulated surface current distribution of the proposed MIMO antenna at 8.5 GHz is shown in Fig. 10. It is found that the current distribution is uniform throughout the patch area, with the exception of the patch element in the middle, and this validates the gain of the antenna.

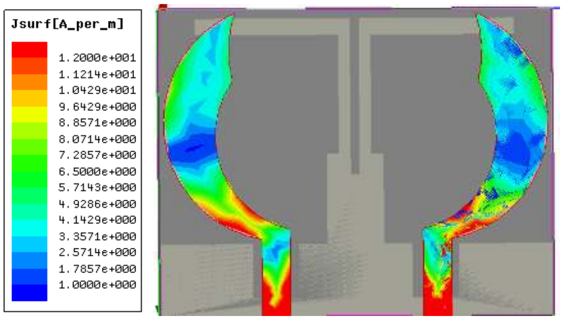

FIGURE 10. **Simulated surface current distribution at 8.5 GHz.**

III. RESULTS DISCUSSION

A. S-PARAMETERS AND AXIAL RATIO

The performance of the proposed textile MIMO antenna is measured using an Anritsu MS2038C vector network analyzer.

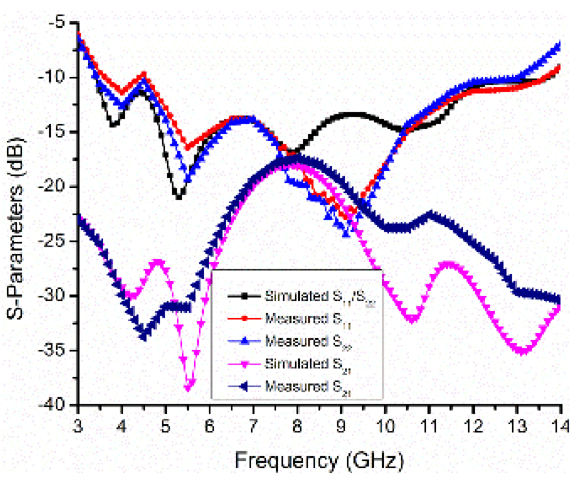

(a)

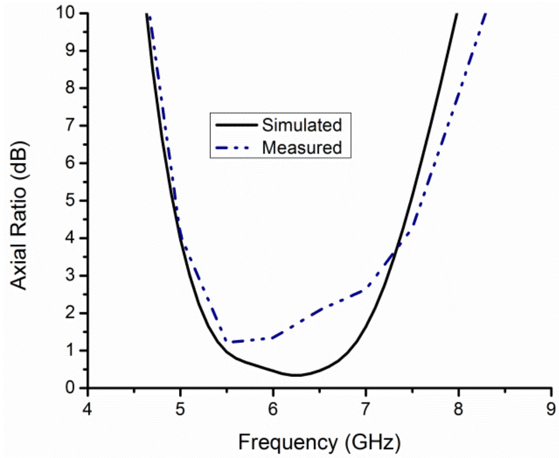

(b)

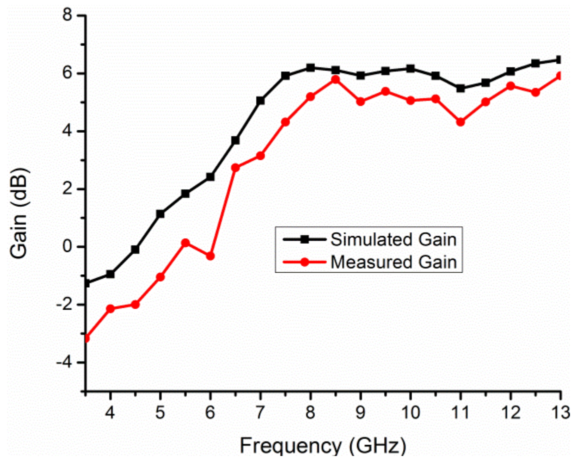

(c)

FIGURE 11. **Simulated and measured response of the textile MIMO antenna: (a) S-parameters, (b) axial ratio, (c) gain.**

The measured and simulated reflection coefficients of the textile MIMO antenna are shown in Fig. 11(a). The measured and simulated -10 dB impedance bandwidths are 113 % (3.6–13 GHz) and 121 % (3.3–13.6 GHz), respectively. As shown in Fig. 11(a), the measured isolation between port-1 and port-2 is >17 dB while the simulated isolation is >19 dB. Since coupling is stronger at lower frequencies, the decoupling structure is designed for a frequency range of 4-6 GHz.

The measured and simulated axial ratio plots (in the broadside direction) of the textile MIMO antenna are illustrated in Fig. 11(b). The measured 3-dB ARBW is 30 % (5.2–7.1 GHz) and the simulated 3-dB ARBW is 37 % (5–7.3 GHz). The minimum (measured) value of the axial ratio is 1.2 dB at 5.2 GHz.

The measured and simulated gain plots of the proposed textile antenna are shown in Fig. 11(c). The measured peak gain is 5.7 dB at 8.5 GHz. The simulated and measured outcomes of the textile antenna are in good agreement. A

This article has been accepted for publication in a future issue of this journal, but has not been fully edited. Content may change prior to final publication. Citation information: DOI 10.1109/ACCESS.2021.3101441, IEEE Access

small difference exists due to the fabrication error and the adhesive used to join the textile materials and the copper part.

B. RADIATION PERFORMANCE

Fig. 12 illustrates the measured and simulated radiation patterns of the proposed CP textile MIMO antenna at 5.3 GHz and 6.3 GHz. The MIMO antenna shows LHCP characteristics when port-1 is excited and port-2 is matched with a load of 50 Ω. In the same way, the MIMO antenna shows RHCP behavior when port-2 is excited and port-1 is matched with a load of 50 Ω. The radiation patterns in Figs. 12(a)–(d) validate the dual-sense behavior of the proposed CP textile MIMO antenna.

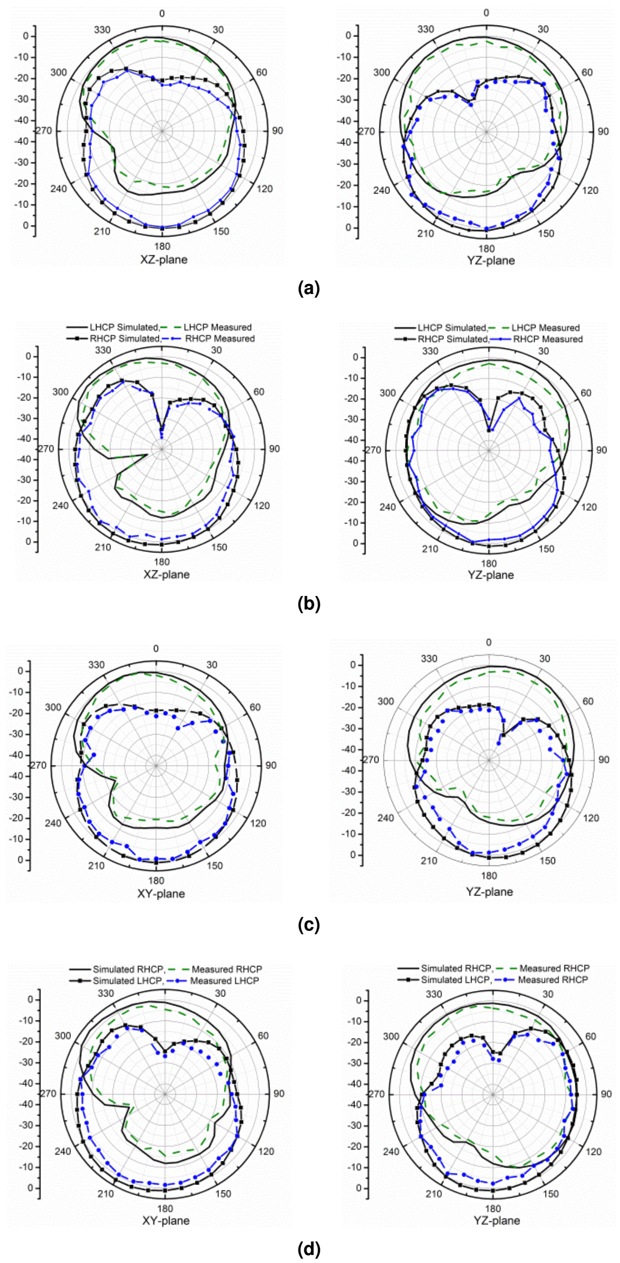

FIGURE 12. Measured and simulated radiation patterns: (a) 5.3 GHz/port-1, (b) 6.3 GHz/port-1, (c) 5.3 GHz/port-2, (d) 6.3 GHz/port-2.

C. MIMO PERFORMANCE

To support the proposed textile antenna diversity performance, MIMO parameters such as envelope correlation coefficient (ECC), diversity gain (DG), total active reflection coefficient (TARC), channel capacity loss (CCL), and mean effective gain (MEG) are evaluated. ECC <0.5, DG >9.95, TARC <0 dB, CCL <0.4 b/s/Hz, and MEG ratio between 0 and -3 dB are required for efficient MIMO system operation [22–25].

1) ECC AND DG

In MIMO systems, ECC demonstrates the correlation between antenna ports. The following relation can be used to evaluate the ECC [25].

$$\text{ECC} = \frac{|S_{11}{}^{*}S_{12} + S_{21}{}^{*}S_{22}|}{(1-|S_{11}|^2-|S_{21}|^2)(1-|S_{22}|^2-|S_{12}|^2)} \quad (1)$$

The simulated and measured ECC curves of the presented textile MIMO antenna are displayed in Fig. 13(a). The ECC between antenna elements-1 and -2 is less than 0.02.

Another important MIMO parameter is DG, which can be calculated using the following relation.

$$\text{DG} = 10\sqrt{1-\text{ECC}^2} \quad (2)$$

The simulated and measured DG curves of the proposed textile MIMO antenna are shown in Fig. 13(a). The DG of the textile antenna is greater than 9.96 dB.

2) TARC

When the antenna elements in a multi-port antenna system operate concurrently, they affect each other's performance. TARC takes into account this effect, which is defined as the square root of the ratio of total incident power to reflected power in the overall MIMO system. The following equation can be used to compute the TARC of the proposed two-port MIMO antenna [26].

$$\text{TARC} = \frac{\sqrt{(S_{11}+S_{22})^2+(S_{21}+S_{12})^2}}{\sqrt{2}} \quad (3)$$

The simulated and measured TARC curves are presented in Fig. 13(b). Here, the measured and simulated TARC values are less than -10 dB for the entire operating band.

3) CCL AND MEG

CCL is the knowledge of the maximum cut-off on the message transmission rate over a communication channel, and it can be evaluated as [25].

$$C\,(loss) = -\log_2 det(\beta^R) \quad (4)$$

This article has been accepted for publication in a future issue of this journal, but has not been fully edited. Content may change prior to final publication. Citation information: DOI 10.1109/ACCESS.2021.3101441, IEEE Access

where $\beta^R = \begin{bmatrix} R_{11} & R_{12} \\ R_{21} & R_{22} \end{bmatrix}$, $R_{ii} = 1 - (|S_{11}|^2 + |S_{22}|^2)$ and

$R_{ij} = -\left(S^*_{ii}S_{ij} + S^*_{ji}S_{jj}\right)$ for $i, j = 1$ or 2

The measured and simulated CCL curves of the proposed textile MIMO antenna are presented in Fig. 14(a). The CCL values are less than 0.2 b/s/Hz for the entire operating band.

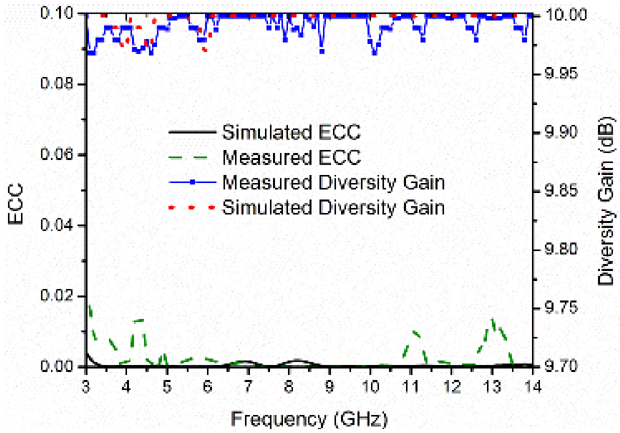

(a)

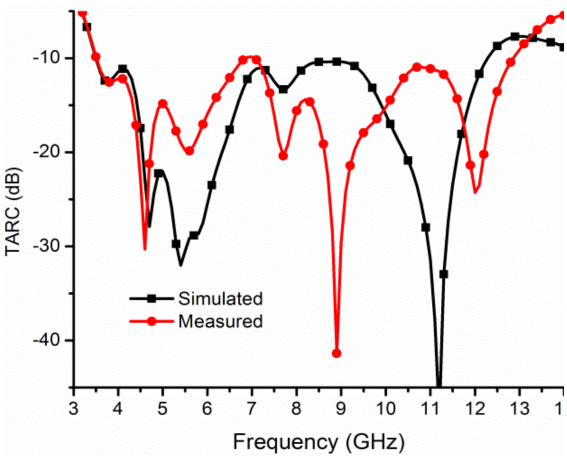

(b)

FIGURE 13. Diversity performance of the textile MIMO antenna: (a) ECC and DG, (b) TARC.

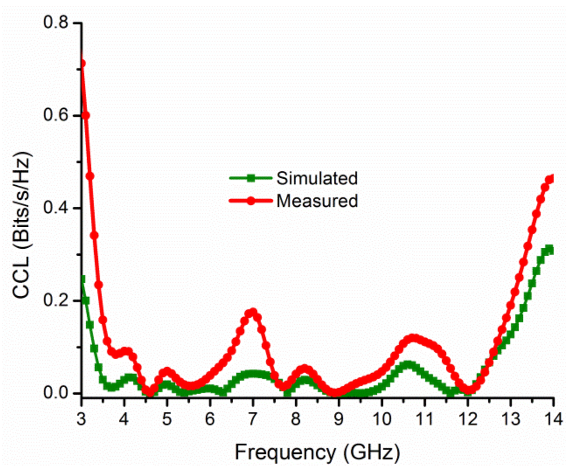

(a)

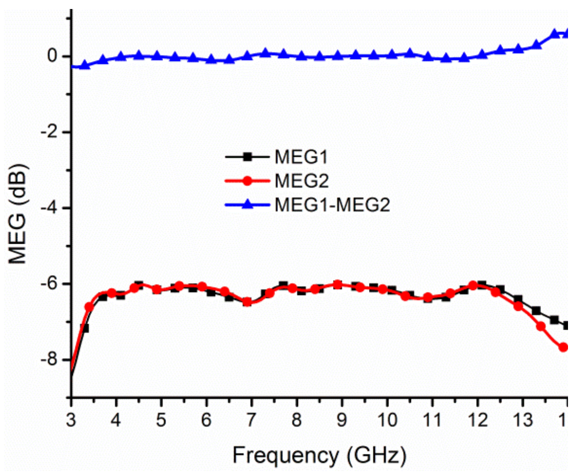

(b)

FIGURE 14. Proposed textile MIMO antenna: (a) CCL, (b) MEG.

MEG reflects gain behavior of the MIMO antenna. It demonstrates that the impact of the wireless environment on diversity has been considered. The following equations can be used to compute the MEG [22].

$$MEG_1 = 0.5\eta_{1,rad} = 0.5[1 - |S_{11}|^2 - |S_{12}|^2] \quad (5)$$

$$MEG_2 = 0.5\eta_{2,rad} = 0.5[1 - |S_{12}|^2 - |S_{22}|^2] \quad (6)$$

The measured MEG graphs of the proposed textile MIMO antenna are plotted in Fig. 14(b). It is noticed that the difference between MEG_1 and MEG_2 is ±0.5 dB.

IV. BENDING ANALYSIS

The wearable antenna may bend when mounted in garments worn on the human body, such as the arms and thighs. To ensure the structural integrity of the antenna, simulations were run to test its ability to bend along the E-plane or H-plane at different radii, 15 mm, 25 mm, 35 mm, and 45 mm. The simulated S_{11} and axial ratio results of the textile MIMO antenna at different bending radii are shown in Figs. 15 and 16, respectively. For better realization, the MIMO antenna is analyzed in two states: bending along the E-plane and bending along the H-plane. Figs. 15(a) and (b) show the simulated results for the E-plane and H-plane bending with radius varying from 15 mm to 45 mm in comparison to the original antenna. It is noticed that the curves are shifted to the higher frequency side by approximately 700 MHz in comparison to the original results.

The MIMO antenna performs well under bend conditions and exhibits a similar bandwidth, however, as the bending radius decreases, the S_{11} results deteriorate due to

This article has been accepted for publication in a future issue of this journal, but has not been fully edited. Content may change prior to final publication. Citation information: DOI 10.1109/ACCESS.2021.3101441, IEEE Access

impedance mismatching between the port and feed line. The same trend can be seen in the H-plane bending analyses, with the resonating band shifting to the right as the bending radius decreases.

Fig. 16 shows the simulated axial ratio, for the E-plane bending, with radius varying from 15 mm to 45 mm in comparison to the original antenna. The 3-dB ARBW shifts to the lower side as the bending radius increases, and it degrades at 6 GHz due to the feed line offset. Figs. 17(a) and (b) show the measured S_{11} and axial ratio of the proposed textile antenna in the E-plane, respectively, and the simulated and measured results are found to be in good agreement.

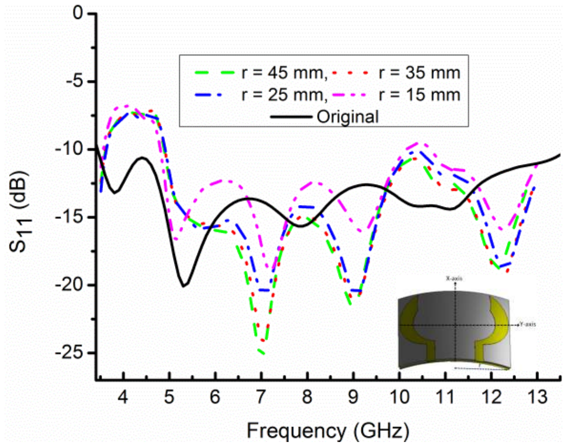

(a)

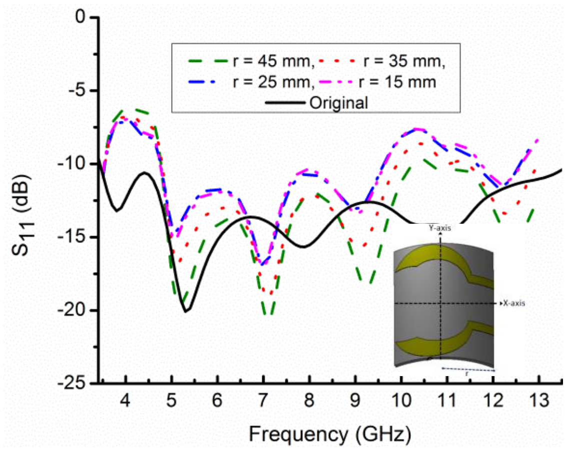

(b)

FIGURE 15. S_{11} comparison for different bending radii: (a) E-plane, (b) H-plane.

Also, the diversity performance of the MIMO antenna is investigated in terms of ECC, DG, MEG, TARC, and CCL in various bending situations, as shown in Table III. It has been found that as the bending radius increases, the performance of the antenna slightly decreases due to changes in the current distribution on the ground plane of the antenna.

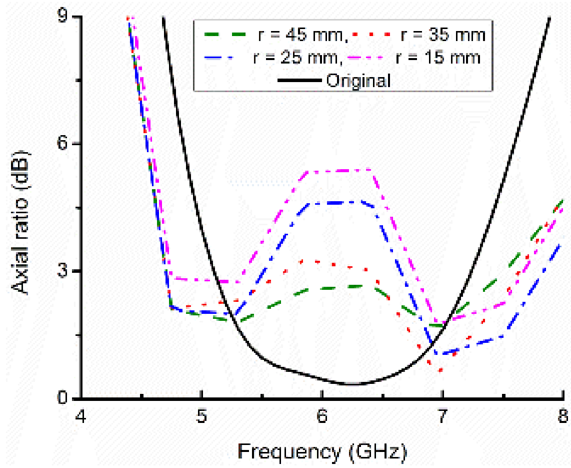

FIGURE 16. Axial ratio comparison for different bending radii in the E-plane.

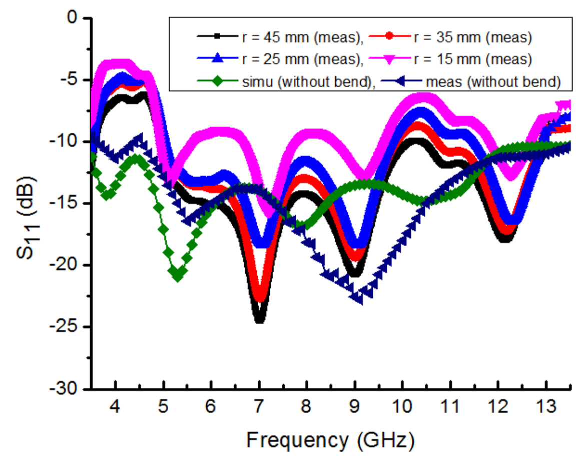

(a)

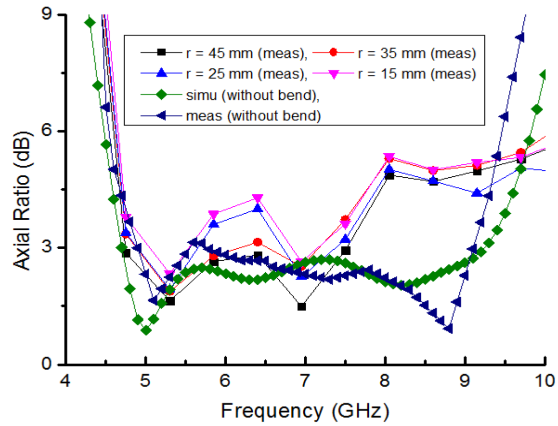

(b)

FIGURE 17. Performance comparison for different bending radii in the E-plane: (a) S_{11}, (b) axial ratio.

Furthermore, the on-body analysis of the antenna is also studied. Table IV shows the intrinsic values of conductivity, permittivity, density, and loss tangent of skin, fat, muscle and bone of a four-layer human arm shown in Fig. 18(a). The simulated S_{11} results for different bending radius are shown in Fig. 18(b), and it is noticed that the curves are shifted slightly towards the right side due to the lossy nature of the human arm and the reduction in the current path length.

TABLE III
DIVERSITY PERFORMANCE OF THE MIMO ANTENNA FOR DIFFERENT BENDING RADII

Bending radius (mm)	Parameters				
	ECC	DG (dB)	MEG1-MEG2 (dB)	TARC (dB)	CCL (b/s/Hz)
45	0.021	9.95	±0.5	-10	0.2
35	0.022	9.93	±0.5	-10	0.2
25	0.023	9.93	±0.5	-9.7	0.22
15	0.023	9.91	±0.5	-9.5	0.23

TABLE IV
INTRINSIC PROPERTIES OF HUMAN TISSUES AT 5.8 GHZ

Properties/Tissues	Skin	Fat	Muscle	Bone
Permittivity (ε_r)	35.1	4.95	48.48	10.3
Conductivity (S/m)	3.71	0.29	4.96	4.56
Loss tangent	0.2835	0.19382	0.24191	0.25244
Density (kg/m^3)	1100	910	1060	1850

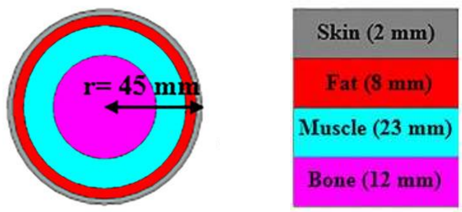

(a)

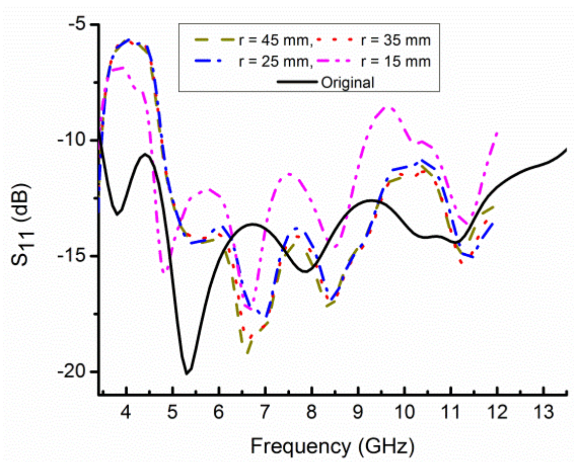

(b)

FIGURE 18. On-body performance of the antenna: (a) four-layer tissue model, (b) S_{11} comparison for different bending radii in the E-plane.

V. SPECIFIC ABSORPTION RATE CHARACTERISTICS

The specific absorption rate (SAR) can be defined by the following relation [27].

$$\mathrm{SAR} = \frac{d}{dt}\left(\frac{dE}{dm}\right) = \frac{d}{dt}\left(\frac{dE}{\rho.dA}\right)\left({}^{W}/_{Kg}\right) \qquad (7)$$

where dm is the incremental mass, dE is the time derivative of the incremental energy, dA is the volume element, and ρ is the mass density. The SAR values are specified by the Federal Communications Commission (FCC), International Commission on Non-Ionizing Radiation Protection (ICNIRP), and IEEE C95.1-2005 standards [28–30]. For 1 W of input power, the maximum SAR value obtained for 10 g of tissue is 5.434 W/kg.

According to the new guidelines, the majority of devices for human body applications require mW power range. The calculated maximum input power of the antenna is 367.86 mW for 10 g of tissue at 2 W input power, which is less than the maximum standard limit. Thus, the proposed antenna will operate within allowable limits.

Table V compares the proposed textile MIMO antenna and recently reported textile/wearable antennas. The parameters compared are antenna size, substrate material, operating bandwidth, fractional bandwidth, gain, ARBW, sense of polarization, and isolation. The wearable antennas presented in [12–16] were LP. The antenna proposed in [11] showed circular polarization behavior, and [17–21] were CP with dual sense, but they showed a small operating bandwidth. In contrast to the reported antenna designs, the proposed textile MIMO antenna exhibits small size, wider axial ratio and impedance bandwidths, and dual-sense (LHCP/RHCP) behavior.

VI. CONCLUSION

In this paper, a wideband CP two-port textile MIMO antenna is proposed. The overall size of the textile antenna is 32.5×42×1 mm^3. The proposed MIMO antenna exhibits an impedance bandwidth of 113 % and ARBW of 30 %. The antenna shows DG >9.96 dB, ECC <0.02, and CCL <0.2 b/s/Hz. The isolation obtained is greater than 18 dB without the use of any additional decoupling elements. SAR analysis of the proposed antenna is also studied for human tissue models and it is found within the acceptable range. The presented antenna is useful for off-body and on-body WLAN, Wi-MAX, and C-band uplink/downlink applications.

ACKNOWLEDGMENT

This research was funded by the Deanship of Scientific Research at Princess Nourah bint Abdulrahman University through the Fast-track Research Funding Program.

TABLE V
COMPARATIVE ANALYSIS OF THE PROPOSED WORK WITH THE REPORTED WEARABLE MIMO ANTENNAS

Ref.	Antenna size (mm^2)	Substrate material (ε_r)	Operating bandwidth (GHz)	Fractional bandwidth (%)	ARBW (GHz)	Gain (dB)	Dual sense	Isolation (dB)
[11]	40 × 40	FR-4 (1.6)	1.6–3.8	92.08	1.8–3.1	2.36	No	>24
[12]	92.3 × 101.6	Textile (1.3)	2.367–2.53, 5.14–5.86	6.65, 13.09	---	5.8	No	>20
[13]	$\pi(21.1)^2$	FR-4 (1.6)	2.4–2.49	3.68	---	4.2	No	>15
[14]	38.1 × 38.1	Textile (1.2)	2.3–2.8	19.6	---	2.79	No	>12
[15]	55 × 35	Jeans (1.6)	2.64–12.28	129.22	---	6.9	No	>26
[16]	70 × 40	Jeans (1.6)	2.4–8	107.69	---	4.4	No	>22
[17]	60 × 60	FR-4 (1.6)	2.0–4.76	81.65	2.0–3.7	4	Yes	>15
[18]	32 × 32	FR-4 (1.6)	1.4–8.73	144.71	3.74–8.8	3.8	Yes	>20
[19]	13.7 × 36.2	Rogers RO4003C (3.38)	5.2–6.3	19.13	5.2–6.3	5.8	Yes	>22
[20]	100 × 150	Rogers RO4350B (3.66)	2.47–2.55	3.2	2.5–2.66	6.1	Yes	>20
[21]	30 × 30	FR-4 (1.6)	2.37–2.54	6.92	2.4–2.5	---	Yes	>20
Prop.	42 × 32.5	Textile (1.34)	3.6–13	113.25	5.2–7.1	5.7	Yes	>18

REFERENCES

[1] Y. S. Chen and T.-Y. Ku, "A low-profile wearable antenna using a miniature high impedance surface for smartwatch applications," *IEEE Antennas Wireless Propag. Lett.*, vol. 15, pp. 1144–1147, 2016.

[2] R. Salvado, C. Loss, R. Gonçalves, and P. Pinho, "Textile materials for the design of wearable antennas: A survey," *Sensors*, vol. 12, no. 11, pp. 15841–15857, 2012.

[3] P. Nepa and H. Rogier, "Wearable antennas for off-body radio links at VHF and UHF bands: Challenges, the state of the art, and future trends below 1 GHz," *IEEE Antennas Propag. Mag.*, vol. 57, no. 5, pp. 30–52, 2015.

[4] B. Hu, G.-P. Gao, L.-L. He, X.-D. Cong, and J.-N. Zhao, "Bending and on-arm effects on a wearable antenna for 2.45 GHz body area network," *IEEE Antennas Wireless Propag. Lett.*, vol. 15, pp. 378–381, 2016.

[5] K. N. Paracha, S. K. Abdul Rahim, P. J. Soh, and M. Khalily, "Wearable antennas: A review of materials, structures, and innovative features for autonomous communication and sensing," *IEEE Access*, vol. 7, pp. 56694–56712, 2019.

[6] M. Klemm, I. Locher, and G. Tröster, "A novel circularly polarized textile antenna for wearable applications," *Proc. 7th Europ. Microw. Week*, pp. 137–140, 2004.

[7] Z. H. Jiang, Z. Cui, T. Yue, Y. Zhu, and D. H. Werner, "Compact, highly efficient, and fully flexible circularly polarized antenna enabled by silver nanowires for wireless body-area networks," *IEEE Trans. Biomed. Circuits Syst.*, vol. 11, no. 4, pp. 920–932, 2017.

[8] Z. H. Jiang and D. H. Werner, "A compact wideband circularly polarized co-designed filtering antenna and its application for wearable devices with low SAR," *IEEE Trans. Antennas Propag.*, vol. 63, no. 9, pp. 3808–3818, 2015.

[9] F. A. Dicandia, S. Genovesi, and A. Monorchio, "Analysis of the performance enhancement of MIMO systems employing circular polarization," *IEEE Trans. Antennas Propag.*, vol. 65, no. 9, pp. 4824–4835, 2017.

[10] H. Li, J. Xiong, Z. Ying, and S. L. He, "Compact and low profile co-located MIMO antenna structure with polarisation diversity and high port isolation," *Electron. Lett.*, vol. 46, no. 2, pp. 108–110, 2010.

[11] A. Iqbal, A. Smida, A. J. Alazemi, M. I. Waly, N. Khaddaj Mallat, and S. Kim, "Wideband circularly polarized MIMO antenna for high data wearable biotelemetric devices," *IEEE Access*, vol. 8, pp. 17935–17944, 2020.

[12] S. Yan, P. J. Soh, and G. A. E. Vandenbosch, "Dual-band textile MIMO antenna based on substrate-integrated waveguide (SIW) technology," *IEEE Trans. Antennas Propag.*, vol. 63, no. 11, pp. 4640–4647, 2015.

[13] D. Wen, Y. Hao, M. O. Munoz, H. Wang, and H. Zhou, "A compact and low-profile MIMO antenna using a miniature circular high-impedance surface for wearable applications," *IEEE Trans. Antennas Propag.*, vol. 66, no. 1, pp. 96–104, 2018.

[14] H. Li, S. Sun, B. Wang, and F. Wu, "Design of compact single-layer textile MIMO antenna for wearable applications," *IEEE Trans. Antennas Propag.*, vol. 66, no. 6, pp. 3136–3141, 2018.

[15] A. K. Biswas and U. Chakraborty, "Compact wearable MIMO antenna with improved port isolation for ultra-wideband applications," *IET Microw. Antennas Propag.*, vol. 13, no. 4, pp. 498–504, 2019.

[16] A. K. Biswas and U. Chakraborty, "A compact wide band textile MIMO antenna with very low mutual coupling for wearable applications," *Int. J. RF Microw. Comput. Eng.*, vol. 29, no. 8, e21769, 2019.

[17] R. K. Saini and S. Dwari, "A broadband dual circularly polarized square slot antenna," *IEEE Trans. Antennas Propag.*, vol. 64, no. 1, pp. 290-294, 2015.

[18] D. S. Chandu and S. S. Karthikeyan, "A novel broadband dual circularly polarized microstrip-fed monopole antenna," *IEEE Trans. Antennas Propag.*, vol. 65, no. 3, pp. 1410-1415, 2017.

[19] M. Y. Jamal, M. Li, and K. L. Yeung, "Isolation enhancement of closely packed dual circularly polarized MIMO antenna using hybrid technique," *IEEE Access*, vol. 8, pp. 11241-11247, 2020.

[20] U. Ullah, I. B. Mabrouk, and S. Koziel, "Enhanced-performance circularly polarized MIMO antenna with polarization/pattern diversity," *IEEE Access*, vol. 8, pp. 11887-11895, 2020.

[21] L. Qu, H. Piao, Y. Qu, H. Kim, and H. Kim, "Circularly polarised MIMO ground radiation antennas for wearable devices," *Electron. Lett.*, vol. 54, no. 4, pp. 189–190, 2018.

[22] J. Nasir, M. H. Jamaluddin, M. Khalily, M. R. Kamarudin, I. Ullah, and R. Selvaraju, "A reduced size dual port MIMO DRA with high isolation for 4G applications," *Int. J. RF Microw. Comput. Aided Eng.*, vol. 25, no. 6, pp. 495–501, 2015.

[23] S. H. Chae, S. Oh, and S. Park, "Analysis of mutual coupling, correlations, and TARC in WiBro MIMO array antenna," *IEEE Antennas Wireless Propag. Lett.*, vol. 6, pp. 122–125, 2007.

[24] H. S. Singh, G. K. Pandey, P. K. Bharti, and M. K. Meshram, "Design and performance investigation of a low profile MIMO/diversity antenna for WLAN/WiMAX/HIPERLAN applications with high isolation," *Int. J. RF Microw. Comput. Aided Eng.*, vol. 25, no. 6, pp. 510–521, 2015.

[25] Y. K. Choukiker, S. K. Sharma, and S. K. Behera, "Hybrid fractal shape planar monopole antenna covering multiband wireless communications with MIMO implementation for handheld mobile devices," *IEEE Trans. Antennas Propag.*, vol. 62, no. 3, pp. 1483–1488, 2014.

[26] S. I. Jafri, R. Saleem, M. F. Shafique, and A. K. Brown, "Compact reconfigurable multiple-input-multiple-output antenna for ultra wideband applications," *IET Microw. Antennas Propag.*, vol. 10, no. 4, pp. 413–419, 2016.

[27] 'IEEE recommended practice for measurements and computations of radio frequency electromagnetic fields with respect to human exposure to such fields, 100 kHz to 300 GHz', IEEE Standard C95.3-2002, 2002.
[28] W. H. Bailey *et al.*, "Synopsis of IEEE Std C95.1™-2019 "IEEE standard for safety levels with respect to human exposure to electric, magnetic, and electromagnetic fields, 0 Hz to 300 GHz," *IEEE Access*, vol. 7, pp. 171346–171356, 2019.
[29] A. Hirata and S. Kodera, "Difference of ICNIRP guidelines and IEEE C95.1 standard for human protection from radio-frequency exposures," *International Symposium on Electromagnetic Compatibility - EMC EUROPE*, Rome, Italy, pp. 1–5, 2020.
[30] International commission on non-ionizing radiation protection (ICNIRP)[1] guidelines for limiting exposure to electromagnetic fields (100 kHz to 300 GHz), *Health Physics*, vol. 118, no. 5, pp. 483–524, 2020.

Sanjeev Kumar received the B.Tech. degree in Electronics and Communication Engineering from Rajiv Gandhi Proudyogiki Vishwavidyalaya, Bhopal, India, in 2009, and M.Tech. degree in Microwave Engineering from the Department of Electronics, University of Delhi, India, in 2012. He completed the Ph.D. degree from the Department of Electronics and Communication Engineering, Jaypee University of Engineering and Technology, Guna, India, in 2019. Currently, he is working as a Research Mentor at Accendere Knowledge Management Services Pvt. Ltd. (a subsidiary of CL Educate Ltd.). Earlier, he worked as a Project Fellow at the Defence Research and Development Organization, Delhi, India. He has published more than forty articles in various peer-reviewed journals and conferences. His research interests include RF circuit design, MIMO antenna, and metamaterials.

Durgesh Nandan received the B.Tech. degree in Electronics and Communication Engineering and M.Tech. degree in Microelectronics & VLSI Design from Rajiv Gandhi Proudyogiki Vishwavidyalaya, Bhopal, India, in 2009 and 2013, respectively. He received the Ph.D. degree from the Department of Electronics and Communication Engineering, Jaypee University of Engineering and Technology, Guna, India, in 2018. Currently, he is working as an Account Manager at Accendere Knowledge Management Services Pvt. Ltd. (a subsidiary of CL Educate Ltd.). He has published more than ninety articles in various peer-reviewed journals and conferences. He is a reviewer/TPC member/session chair for more than fifty national/international conferences. He is a co-inventor of one Indian patent, and has published two technical books. He was recognized as "Young Personality of the Year (below 40 years)" by the International Academic and Research Excellence Awards, in 2019. He also received the "I2OR Preeminent Researcher Award 2019" for his remarkable contribution in the field of VLSI and DSP by the International Institute of Organized Research. His research interests include computer arithmetic, microwave & RF, speech processing, the hardware design for big data/AI applications, and the Internet of Things.

Kunal Srivastava received the B.Tech. degree in Electronics and Communication Engineering from Punjab Technical University, Jalandhar, India, and M.Tech. degree in Microwave Electronics from the University of Delhi, India. He received the Ph.D. degree in Electronics Engineering from the Indian Institute of Technology (ISM), Dhanbad, India. His areas of research include the design and development of MIMO, ultra-wideband, and circularly polarized antennas.

Sachin Kumar received the B.Tech. degree from Uttar Pradesh Technical University, Lucknow, India, in 2009, and the M.Tech. and Ph.D. degrees from Guru Gobind Singh Indraprastha University, Delhi, India, in 2011 and 2016, respectively. He is currently a Research Assistant Professor in the Department of Electronics and Communication Engineering, SRM Institute of Science and Technology, Chennai, India. He has published more than ninety research articles in several peer-reviewed international journals and conferences. He is also a frequent reviewer for more than fifty scientific journals and book publishers. He is a recipient of the Teaching-cum-Research Fellowship from the Government of NCT of Delhi, India, and the Brain Korea 21 Plus Research Fellowship from the National Research Foundation of South Korea. He is a member of the Indian Society for Technical Education and the Korean Institute of Electromagnetic Engineering and Science.

Hari Singh received the B.Sc. (Electronics Hons.) degree from Hansraj College, University of Delhi, New Delhi, India, in 2006, and the M.Sc. (Electronics) degree from the Department of Electronic Science, University of Delhi South Campus, New Delhi, India, in 2008. Since 2009, he is working as an Assistant Professor in the Department of Electronic Science, Sri Venkateswara

College, University of Delhi, New Delhi, India. Also, he is working towards his Ph.D. degree from the School of Computation and Integrative Sciences, Jawaharlal Nehru University, New Delhi, India. His areas of research include the design and development of microstrip antennas, circularly polarized antennas, MIMO, and wearable antennas.

Mohamed Marey (SM'14) received the M.Sc. degree in electrical engineering from Menoufia University, Egypt, in 1999, and the Ph.D. degree in electrical engineering from Ghent University, Belgium, in 2008. From 2009 to 2014, he was a Research Associate and a Visiting Professor with the Faculty of Engineering and Applied Science, Memorial University, Canada. He is currently a full Professor with the Faculty of Electronic Engineering, Menoufia University, Egypt. He is on a sabbatical leave in order to join Prince Sultan University, Saudi Arabia, as a research laboratory leader of the smart systems engineering laboratory. He authored the book *Multi-Carrier Receivers in the Presence of Interference: Overlay Systems* (VDM Publishing House Ltd., 2009) and around 100 scientific papers published in international journals and conferences. His main research interests are in wireless communications and digital signal processing, with a particular focus on smart antennas, cooperative communications, signal classification for cognitive radio systems, synchronization and channel estimation, multiple-input multiple-output antenna systems, multicarrier systems, and error correcting codes. He was a recipient of the Young Scientist Award from the International Union of Radio Science in 1999.

Hala Mostafa received the Ph.D. degree in electrical engineering from the Faculty of Engineering and Applied Science, Memorial University, Canada, in 2014. From 2014 to 2015, she was a Research Scientist at Memorial University. She is currently an assistant professor at the Information Technology Department, College of Computer and Information Sciences, Princess Nourah bint Abdulrahman University, Riyadh, Saudi Arabia. Her main research interests are in wireless communications, with a particular focus on smart antennas and wireless sensor networks.

Binod Kumar Kanaujia received the B.Tech. degree in Electronics Engineering from Kamla Nehru Institute of Technology, Sultanpur, India, in 1994, and the M.Tech. and Ph.D. degrees from the Department of Electronics Engineering, Indian Institute of Technology Banaras Hindu University, Varanasi, India, in 1998 and 2004, respectively. He is currently a Professor with the School of Computational & Integrative Sciences, Jawaharlal Nehru University, New Delhi, India. He has been credited to publish more than 350 research articles with more than 2900 citations and h-index of 25 in several peer-reviewed journals and conferences. He had supervised 50 M.Tech. and 15 Ph.D. scholars in the field of RF and microwave engineering. He is currently on the editorial board of several international journals. He is a member of the Institution of Engineers, India, the Indian Society for Technical Education, and the Institute of Electronics and Telecommunication Engineers of India. He had successfully executed five research projects sponsored by several agencies of the Government of India, such as DRDO, DST, AICTE, and ISRO.